



HAL
open science

Regeneration of an Aged Hydrodesulfurization Catalyst by Non-Thermal Plasma: Characterization of Refractory Coke Molecules

Hawraa Srour, Nadia Guignard, Mehrad Tarighi, Elodie Devers, Adrien Mekki-Berrada, Joumana Toufaily, Tayssir Hamieh, Catherine Batiot-Dupeyrat, Ludovic Pinard

► **To cite this version:**

Hawraa Srour, Nadia Guignard, Mehrad Tarighi, Elodie Devers, Adrien Mekki-Berrada, et al.. Regeneration of an Aged Hydrodesulfurization Catalyst by Non-Thermal Plasma: Characterization of Refractory Coke Molecules. *Catalysts*, 2021, 11 (10), pp.1153. 10.3390/catal11101153 . hal-03499605

HAL Id: hal-03499605

<https://ifp.hal.science/hal-03499605>

Submitted on 21 Dec 2021

HAL is a multi-disciplinary open access archive for the deposit and dissemination of scientific research documents, whether they are published or not. The documents may come from teaching and research institutions in France or abroad, or from public or private research centers.

L'archive ouverte pluridisciplinaire **HAL**, est destinée au dépôt et à la diffusion de documents scientifiques de niveau recherche, publiés ou non, émanant des établissements d'enseignement et de recherche français ou étrangers, des laboratoires publics ou privés.



Distributed under a Creative Commons Attribution 4.0 International License

Article

Regeneration of an Aged Hydrodesulfurization Catalyst by Non-Thermal Plasma: Characterization of Refractory Coke Molecules

Hawraa Srour¹, Nadia Guignard¹, Mehrad Tarighi¹, Elodie Devers², Adrien Mekki-Berrada², Joumana Toufaily³ , Tayssir Hamieh^{3,4} , Catherine Batiot-Dupeyrat¹  and Ludovic Pinard^{1,*}

- ¹ Institut de Chimie des Milieux et Matériaux de Poitiers (IC2MP), UMR 7285 CNRS, 4 rue Michel Brunet, Bâtiment B27, TSA 51106, CEDEX 9, 86073 Poitiers, France; hawraa.srour@univ-poitiers.fr (H.S.); nadia.guignard@univ-poitiers.fr (N.G.); mehrad.tarighi@univ-poitiers.fr (M.T.); catherine.batiot.dupeyrat@univ-poitiers.fr (C.B.-D.)
- ² IFP Energies nouvelles, Rond-Point de l'échangeur de Solaize, BP 3, 69360 Solaize, France; elodie.devers@ifpen.fr (E.D.); adrien.mekki-berrada@ifpen.fr (A.M.-B.)
- ³ Laboratory of Materials, Catalysis, Environment and Analytical Methods Laboratory (MCEMA), Faculty of Sciences, Lebanese University, Hadath 6573/14, Lebanon; joumana.toufaily@ul.edu.lb (J.T.); tayssir.hamieh@ul.edu.lb (T.H.)
- ⁴ Faculty of Science and Engineering, Maastricht University, P.O. Box 616, 6200 MD Maastricht, The Netherlands; t.hamieh@maastrichtuniversity.nl
- * Correspondence: ludovic.pinard@univ-poitiers.fr



Citation: Srour, H.; Guignard, N.; Tarighi, M.; Devers, E.; Mekki-Berrada, A.; Toufaily, J.; Hamieh, T.; Batiot-Dupeyrat, C.; Pinard, L. Regeneration of an Aged Hydrodesulfurization Catalyst by Non-Thermal Plasma: Characterization of Refractory Coke Molecules. *Catalysts* **2021**, *11*, 1153. <https://doi.org/10.3390/catal11101153>

Academic Editor: Luciana Lisi

Received: 22 August 2021

Accepted: 24 September 2021

Published: 25 September 2021

Publisher's Note: MDPI stays neutral with regard to jurisdictional claims in published maps and institutional affiliations.



Copyright: © 2021 by the authors. Licensee MDPI, Basel, Switzerland. This article is an open access article distributed under the terms and conditions of the Creative Commons Attribution (CC BY) license (<https://creativecommons.org/licenses/by/4.0/>).

Abstract: This study describes the phenomena involved during the regeneration of an aged industrial hydrodesulfurization catalyst (CoMoP/Al₂O₃) using a non-thermal plasma at a low temperature (200 °C). The changes occurring during regeneration were studied by characterizing spent, partially, and fully regenerated catalysts by XRD, Raman, TEM spectroscopy, and the coke deposited on the catalyst surface by Laser desorption/ionization time-of-flight mass spectrometry (LDI TOF/MS). The coke is a mixture of several polycyclic molecules, the heaviest with a coronene backbone, containing up to seven sulfur atoms. This kinetic study shows that the oxidation rate depends on the nature of the coke. Hence, explaining the formation of VOCs from heavy polycyclic carbon molecules without complete oxidation to CO₂. However, XRD and Raman spectroscopies evidence CoMoO₄ formation after a long treatment time, indicating hot spots during the regeneration.

Keywords: HDS catalyst; thermal regeneration; non-thermal plasma; coke

1. Introduction

Non-thermal plasma (NTP) attracts a lot of interest because this technology is capable of carrying out thermodynamically unfavorable reactions, for example, hydrocarbons reforming [1], CO₂ hydrogenation, ammonia synthesis [2], and VOCs elimination [3,4]. The combination with plasma and catalysis has been largely described to perform many reactions [5,6]; some studies were also reporting using plasma to prepare [7] and regenerate catalysts [8,9]. Indeed, as indicated in the paper: “The 2020 plasma catalysis roadmap” [5], non-thermal plasma treatment appears as an effective technique for removing coke from various spent catalysts.

The main advantage of oxygen plasma is that it creates O-atoms through simple dissociation of O₂ by electron collisions, the active species being: O₂⁺, O⁻, O₂⁻ and O₃⁻ [10]. Using a noble gas such as argon or helium with oxygen is particularly effective for catalyst decoking, as shown by Khan and Al Jalal [11]. The authors showed that atomization of O₂ was improved with He and Ar compared to N₂, most probably due to reactions between O atoms and N forming species such as NO, NO₂, N₂O, and N₂O₅.

The elimination of coke from a zeolite was reported using a glow discharge [12] or a dielectric barrier discharge (DBD) [13]. This technology efficiently removes carbon deposits on a spent H-ZSM-5 zeolite. A Pt-Sn/Al₂O₃ catalyst was also decoked successfully in a

pin to plate dielectric barrier discharge (DBD) plasma [14]. In previous papers using a DBD pin to plate geometry and a bi-polar pulse generator, we performed the complete regeneration of a coked H-ZSM-5 (MFI) zeolite [15]. We showed that the active oxygen species formed under plasma discharge could diffuse within the microporosity of zeolite. Later, a cylindrical fixed-bed reactor was used to study the regeneration of FAU zeolite. After two hours of plasma treatment, at room temperature with a deposited power of 12 W, the micropore volume was fully restored [16].

The regeneration of aged industrial hydrodesulfurization (HDS) catalyst by non-thermal plasma was also examined [17]. The study was performed using the most employed catalyst in the HDS process, cobalt–molybdenum supported on alumina after a sulfidation step, called “CoMo” [18]. The conventional method for HDS catalyst regeneration is an optimized thermal treatment that does not exceed 500 °C to minimize the formation of crystallized species like CoMoO_4 or CoAl_2O_4 known to limit the HDS activity, such as [18]. Nevertheless, the conventional regeneration process only partially restores the catalytic activity to a level of 70–90% [19]. Thus, searching for alternative technologies is of particular importance. Recently, we compared the regeneration efficiency of an aged industrial hydrodesulfurization catalyst ($\text{CoMoP}/\text{Al}_2\text{O}_3$) by thermal oxidation with non-thermal plasma technology (NTP) [20]. Complete regeneration of the HDS catalyst by NTP required heating the dielectric barrier discharge plasma reactor to a temperature that is still much lower than that used for total coke removal by the conventional route. Complete coke removal is achieved with an NTP from 250 °C. Since the coke elimination is partial at low temperatures, this suggests the presence of coke molecules refractory to the NTP treatment. We have also found that the regeneration of an aged HDS catalyst by non-thermal plasma is much more complicated than a coked zeolite [17]. On the other side, a higher temperature is required for the thermal combustion of coke on a microporous catalyst than on an alumina-based catalyst. These differences would indicate that the efficiency of the NTP process depends more on the nature of the carbonaceous compounds deposited on the surface of the catalyst than on their location.

The chemical composition of coke on HDS catalyst is rarely studied owing to its complexity. Extensive characterization of these heavy coke molecules (molar weight > 300 g/mol) is limited due to their lack of solubility in the most common solvents [21]. Significant advances have been made through the use of matrix-assisted laser desorption/ionization time-of-flight mass spectrometry (MALDI-TOF/MS) [22,23] to characterize heavy coke molecules on zeolite. To our knowledge, this technique has never been used to characterize the HDS catalyst. Yet, Kimura et al. have elucidated the chemical composition and structure of the coke in greater detail using direct analysis in real-time time-of-flight mass spectrometry (DART-TOF/MS) measurements on spent catalysts [24]. The coked catalysts were recovered from an HDS unit of the bench-scale plant for short and long periods, i.e., 160 and 2300 h. The coke on a catalyst used for 160 h was composed of polycyclic aromatic compounds with around 3 to 8 rings. In comparison, a catalyst used for 2300 h was composed of polycyclic aromatic compounds with 2 to 13 rings.

This study aims to characterize in detail the nature of the coke on an industrial HDS catalyst using laser desorption/ionization time-of-flight mass spectrometry (LDI TOF/MS), a technique already used to characterize the external coke present on zeolites. The characterization of the HDS catalyst at different regeneration times by non-thermal plasma will allow the identification of the coke molecules refractory to regeneration and the mechanisms involved during regeneration

2. Results and Discussion

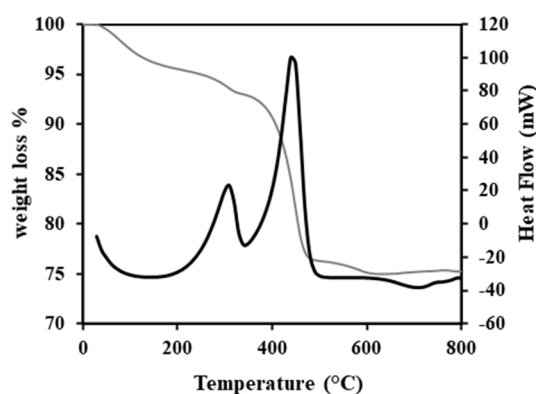
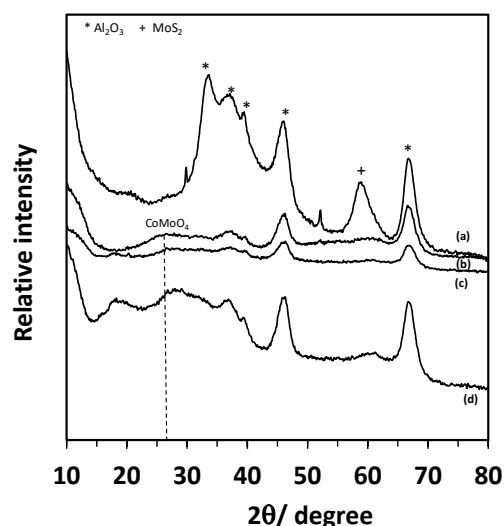
2.1. Characterization of the Spent Catalyst

The carbon content on the spent catalyst determined by elementary analysis is 13.0 wt.% (Table 1), while the sulfur content, derived mainly from the remaining sulfur phase, i.e., CoMoS , MoS_2 , Co_9S_8 , is 8.8 wt.% [25].

Table 1. Composition of the spent catalyst and extracted coke.

Oxide/Element (wt.%)	P ₂ O ₅	MoO ₃	CoO	C	S
Spent catalyst	5.2	20.3	4.0	13.0	8.8
Extracted coke	-	14.0	0.6	15.1	4.9

TGA profile of the spent catalyst, shown in Figure 1, exhibits two-weight losses accompanied by two exothermic maxima at 310 and 440 °C, respectively. The first loss (2.4 wt.%) corresponds to the formation of SO₂ and eventually to the combustion of “soft” coke localized at the surface or the vicinity of MoS₂ slabs. In contrast, the second loss at 440 °C (16.9 wt.%) corresponds to the “hard” coke localized at the surface of the alumina [26,27]. The mass loss observed on TGA is more significant than the sample carbon content. The weight difference is attributed to the sulfur atoms in the coke and to MoS₂ slabs decomposition suggesting that one part of coke molecules contain sulfur atoms; the other part also corresponds to the decomposition of the MoS₂ slabs. Indeed, the characteristic Bragg peaks of MoS₂ at $2\tau = 59^\circ$ can be seen in Figure 2, as well as the characteristics peaks of Al₂O₃, i.e., $2\theta = 33.4^\circ, 37^\circ, 39.5^\circ, 46.1^\circ$ and 66.7° .

**Figure 1.** TGA profile of the spent catalyst.**Figure 2.** XRD patterns of the spent catalyst before (a) and after NTP (non-thermal plasma) treatment were carried out at 7 W at 200 °C during 5 (b), 10 (c) 20 min (d).

TEM micrographs of the spent catalyst shown in Figure 3 display black thread-like fringes, which correspond to molybdenum disulfide MoS₂ slabs [28]. The MoS₂ slabs are homogeneously distributed on the alumina support with a density of 3.5 per 100 nm². The sheet lengths based on 500 slabs counted range from 3 to 13 nm, with a stacking of 1 or 2 slabs and an average size of 6 nm, which is much higher than the average size of 3 nm

observed on fresh sulfide catalyst [29], highlighting the sintering of the active phase during hydrotreating [30].

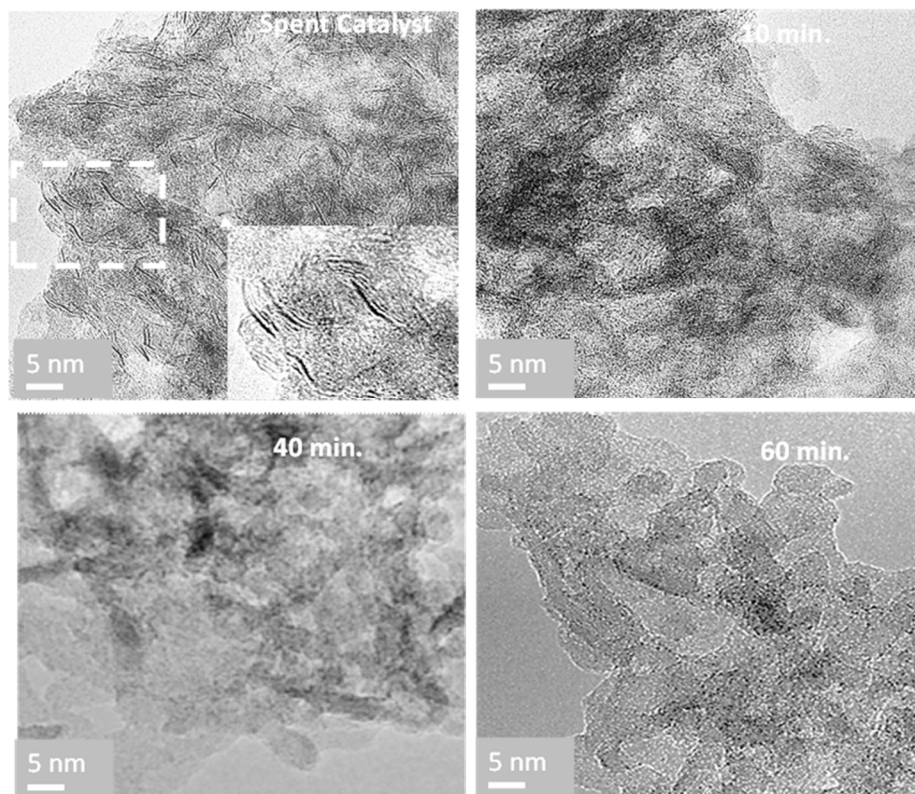


Figure 3. TEM images of the spent catalyst before and after NTP treatment were carried out at 7 W at 200 °C during 10, 40, and 60 min.

Figure 4 (spectrum a) presents the Raman spectrum of the spent catalyst in three regions: 100–500 cm^{-1} , 500–1000 cm^{-1} , and 1000–1800 cm^{-1} , and Table 2 summarizes the assignment of the major peaks. The spent catalysts' spectrum exhibits two peaks at 382 and 407 cm^{-1} , assigned to MoS_2 slabs [31], confirming TEM observations. The two characteristic bands for carbon structures are observed: one is centered at 1605 cm^{-1} and exhibits a Gaussian symmetrical peak, called G band, and one unsymmetrical centered at 1338 cm^{-1} named D band. The deconvolution of these bands allows discriminating four more peaks, as displayed in Figure 5, attributed to an amorphous carbon phase with C sp^3 at 1215 cm^{-1} and C sp^2 at 1550 cm^{-1} , and some defective aspects of graphene (1268 and 1374 cm^{-1}). The graphitization ratio (ID/IG) is calculated using the integrated intensities of the D and G bands (Table 2). This ratio is inversely proportional to the degree of graphitization (Equation (1)) and can be used to evaluate the size of graphitic crystals (L_a) [30].

$$L_a(\text{nm}) = \left(2.4 \times 10^{-10}\right) \times (\lambda_{\text{laser}})^4 \times \frac{IG}{ID} \quad (1)$$

with $\lambda_{\text{laser}} = 532 \text{ nm}$.

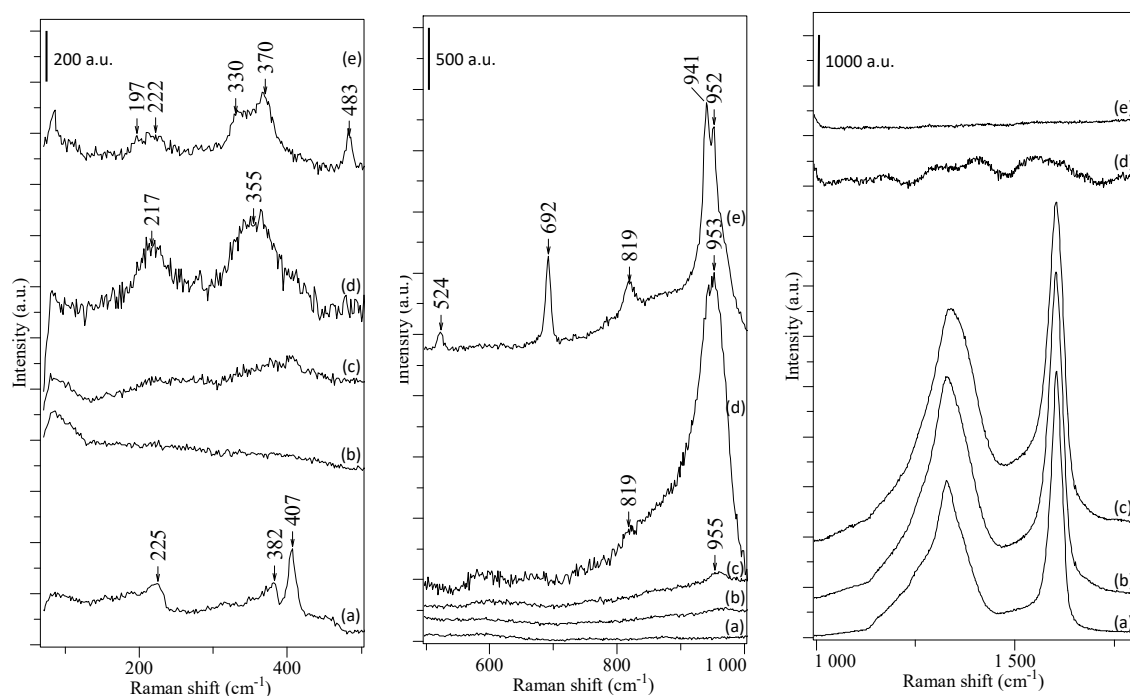


Figure 4. Raman spectrum of the spent catalyst (a) before and after NTP treatment carried out at 7 W at 200 °C during 5 (b), 10 (c) 40 (d), and 60 (e) min.

Table 2. Raman peak positions and assignment of major vibrational bands.

Assignment	Peak Position (cm ⁻¹)	Ref
CoMoO ₄	330, 370, 819, 941, 952	[19,32]
CoMo ₆ or AlMo ₆	217, 351, 376, 573, 909, 952	[19]
Co ₃ O ₄	197, 483, 524, 692	[33]
MoS ₂	225, 382, 405	[28]
Graphitic carbon (G peak)	1580–1600	[29]
Disordered amorphous carbon (D peak)	1338	[29]
Carbon sp ³	1215	[30]
Carbon sp ² (amorphous phase)	1550	[31]

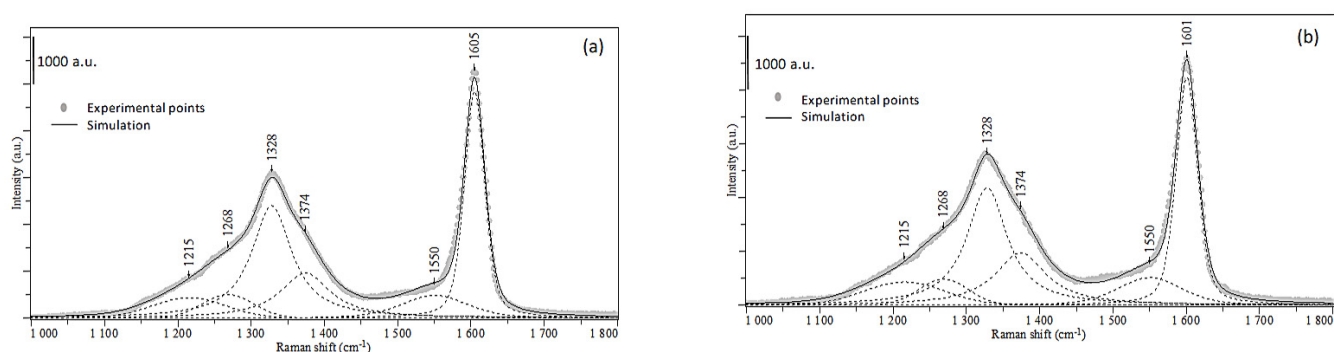


Figure 5. Raman spectrum of the spent catalyst (a) and extracted coke by HF (b), with the corresponding curve fitted bands.

The ID/IG ratio corresponding to the aged HDS catalyst is equal to 1.4., which corresponds to a carbon crystal size of ca. 16 nm.

The mass distribution of the carbonaceous molecules on the catalyst surface is determined by laser desorption-ionization-time of flight mass spectroscopy (LDI-TOF/MS) [34]. Figure 6 displays the LDI-TOF/MS spectrum of the spent catalyst, which exhibits a broad mass distribution ranging between 150 to 550 Da, with a maximum of 228 Da (parent peak).

An example of the skeleton of a light coke molecule with an atomic molar mass of 202, 209 is given in Scheme 1. The number of aromatic rings is in agreement with Kimura et al. [24].

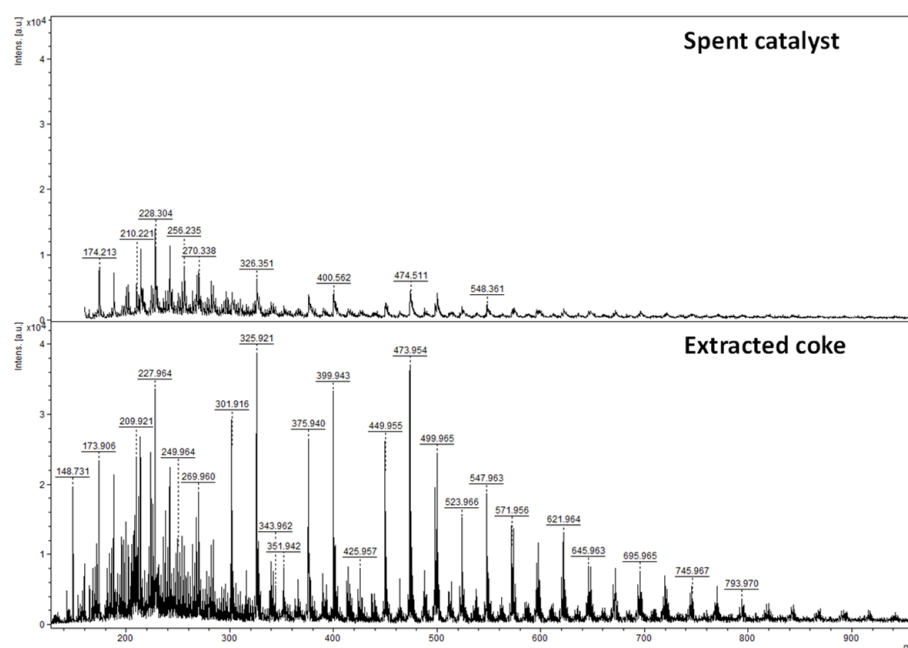
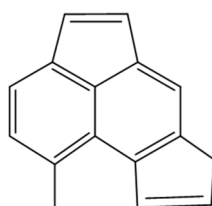


Figure 6. Comparison of LDI-TOF/MS spectrum between the spent catalyst and the extracted coke by HF.



Scheme 1. Example of “light” coke molecule.

Three families with several carbon atoms between 15 and 25 are ranked as a function of their degree of unsaturation (DU). The backbone of each family is more or less alkylated. For example, in a family with a DU of 13, the number of alkyl groups (CH_3) varies from 0 to 7 (Table 3).

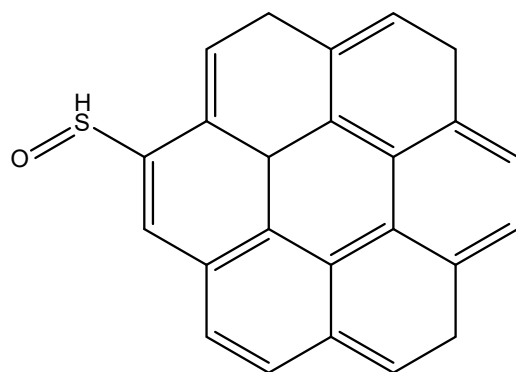
The elemental composition (Table 1) of the extracted coke shows that it is not only composed of carbon (15.1 wt.%) but also sulfur (4.9 wt.%), the content of which is lower on the spent catalyst (8.8 wt.%). The extracted coke also contains a significant amount of MoO_3 (14 wt.%) and, to a lesser extent, CoO (0.6 wt.%). It is worth mentioning that the extract has shades of blue. Cobalt and molybdenum in the extract suggest that some of the coke molecules are strongly bonded to metal atoms.

The Raman spectra of the spent catalyst and extracted coke (Figure 5) show similar D and G bands with an identical ID/IG ratio, revealing that no change occurs during HF extraction. The main difference between the spent catalyst and the extracted coke appears with LDI-TOF/MS analysis (Figure 6). The latter is three times more intense and has a broader mass distribution ranging from 150 to 800 Da. Nevertheless, both spectra have typical families with molar weights ranging from 100 Da to 300 Da and degrees of unsaturation between 8 and 13 ($\text{C}_{15}\text{H}_{14}\text{O}$ - $\text{C}_{25}\text{H}_{26}$, Table 3). These common molecules are referred to as “light” coke. On the extracted coke, relatively heavy coke molecules are detected with a molar weight that can exceed 900 Da. The “heavy” coke has a particular mass distribution with peaks separated by 48.00 Da. This difference does not correspond to two ethylene fragments, but the exact mass indicates that a value of 48.00 is sulfide

oxide (SO). Therefore, the unexpected presence of SO shows that oxidation of the heavy sulfated coke molecules occurs during HF extraction. Some heavy sulfated molecules have a coronene backbone (MW: 354.42 g·mol⁻¹, Scheme 2) substituted up to seven sulfur oxide groups (Table 3).

Table 3. LDI-TOF/MS identification results concerning the chemical composition of the spent catalyst.

Degree of Ensaturation (DU)	Chemical Formula	Number of Alkyl Groups Attached to the Structural Unit	Number of SO Units Attached to the Structural Unit	Molecular Weight (m/z)
Spent catalyst				
9	C ₁₅ H ₁₄ O, C ₁₆ H ₁₆ O,C ₁₇ H ₁₇ O	3, 4 5		210.221, 224.222, 238.251
12	C ₁₆ H ₁₀ , C ₁₇ H ₁₂ , C ₁₈ H ₁₄ , C ₂₀ H ₂₂ , C ₂₁ H ₂₄	0, 1, 2,		202.209, 216.209, 230.229
13	C ₁₈ H ₁₂ , C ₁₉ H ₁₄ , C ₂₀ H ₁₆ , C ₂₁ H ₁₈ , C ₂₂ H ₂₀ , C ₂₅ H ₂₆	0, 1, 2, 3, 4, 7		228.304, 242.306, 256,235, 270.338, 284,380, 326,351
Extracted coke				
8	C ₁₅ H ₁₂ O, C ₁₆ H ₁₄ O, C ₁₇ H ₁₆ O, C ₁₈ H ₁₈ O, C ₁₉ H ₂₀ O	3, 4, 5, 6, 7		208.681, 221.965, 235.937, 249.964, 263.983
9	C ₁₂ H ₈ O, C ₁₃ H ₁₀ O, C ₁₄ H ₁₂ O, C ₁₅ H ₁₄ O, C ₁₆ H ₁₆ O, C ₁₇ H ₁₈ O C ₁₈ H ₂₀ O	0, 1, 2, 3, 4, 5, 6		167.855, 191.877, 195.897, 209.921, 223.944, 237.963, 251.982
11	C ₂₀ H ₂₀ , C ₂₁ H ₂₁	4, 5		259.952, 273.966 199.933, 213.954, 227.964,
13	C ₁₅ H ₆ , C ₁₆ H ₈ , C ₁₇ H ₁₀ , C ₁₈ H ₁₂ , C ₂₀ H ₁₆ , C ₂₁ H ₁₈ , C ₂₂ H ₂₀ , C ₂₅ H ₂₆	0, 1, 2, 3, 5, 6, 7, 10		241.976, 255.976, 269.960, 283.969
	C ₂₃ H ₁₂ O ₂ S, C ₂₃ H ₁₂ O ₃ S ₂ C ₂₄ H ₂₆ O ₃ S ₂ C ₂₄ H ₂₆ O ₄ S ₃ C ₂₃ H ₁₆ O ₅ S ₄ C ₂₃ H ₁₆ O ₆ S ₅ C ₂₃ H ₁₆ O ₇ S ₆ C ₂₃ H ₁₈ O ₆ S ₅ C ₂₃ H ₁₈ O ₇ S ₆ C ₂₃ H ₁₈ O ₈ S ₇	0, 1	1, 2 1, 2, 3 1, 2, 3	351.942, 399.943, 425.957, 473.954 499.965, 547.963, 595.959 549.975, 597.966,645.963



Scheme 2. Example of sulfated “heavy” coke molecule.

Thus, sulfur is present in organic form as traces of heavy sulfated carbonaceous molecules and mainly as MoS₂ slabs.

2.2. Characterization of the Partially and Fully Regenerated HDS Catalyst by Non-Thermal Plasma

The treatment under plasma was performed at room temperature and 200 °C, while the deposited power was fixed at 7 W (frequency = 2 kHz) by adjusting the voltage ($U = 13$ and 11.5 kV at 20 and 200 °C, respectively). A decrease in the gas density as temperature increases explains this adjustment. Figure 7 displays that a rise in temperature from 20 to 200 °C improves the plasma efficiency, the yield into CO_x increased from 18 to 65%, while complete removal of sulfur and carbon is achieved. It is important to note that at 200 °C, no C nor any S are removed by a simple thermal treatment (Figure 2).

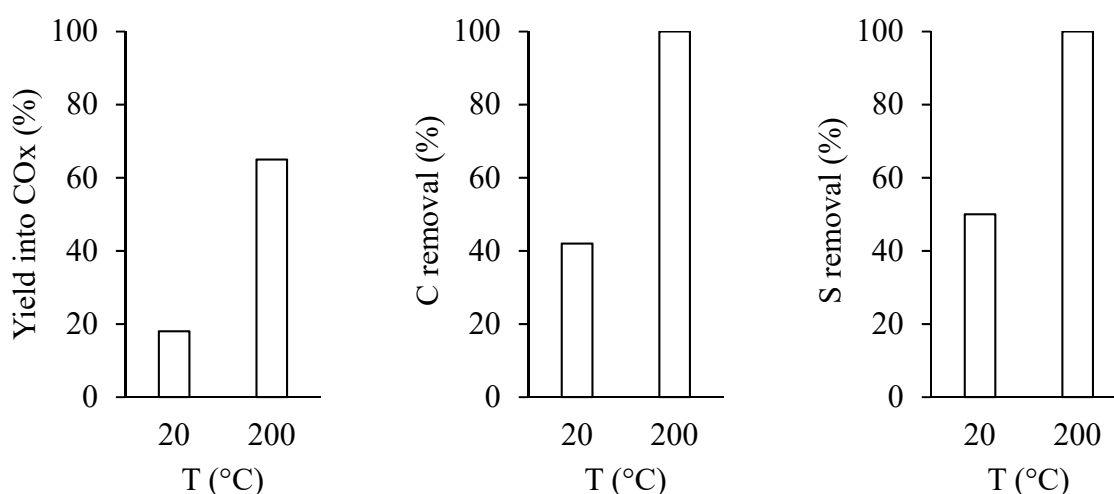


Figure 7. Influence of temperature on the yield into CO_x, C, and S removal after 60 min of plasma treatment at 7 W.

The changes that occur during non-thermal plasma regeneration assisted by moderate heating (200 °C, [20]) were monitored as a function of time. Different durations were selected, i.e., 5, 10, and 40 min, to evaluate the physicochemical alterations of the HDS catalyst and the extracted coke.

Figure 8 compares the CO_x production with the carbon and sulfur removals present on the spent catalyst as a function of treatment time. S removal appears directly after 5 min of treatment, reaching about 80%, while the C removal rate is seven times slower. After 60 min, both S and C are fully removed. The plot of cumulated yields into CO_x exhibits a delayed increase reaching a total of 60% after one hour. This delay is not due to an experimental fact, and the flash evolution of sulfur removal proves that. Up to 10 min of treatment, there is a complete carbon balance and a total selectivity into CO_x. Yet, a change appears after 20 min, with a default in the carbon balance. A difference between C removals and the cumulated yield into CO_x appears and increases, reaching 30% after 60 min at total conversion.

The combustion of coke by plasma begins with the “lightest molecules,” which allow it to be oxidized to CO₂, while the “heaviest” ones lead to incomplete combustion. Indeed, Figure 9 shows that the treatment time impacts the “light coke” more than the “heavy sulfated molecules. The latter are refractory to oxidation. The oxidation rate depends on the nature of the coke. Higher character polycyclic compounds of the coke lower their reactivity relative to the short-lived oxygenated species. Indeed, in the regeneration of a spent zeolite, the coke oxidation begins by total oxidation into CO₂ (and CO) of alkylbenzene then alkyl naphthalene, followed by partial oxidation into volatile organic compounds of pyrene, then coronene [16]. Yet, the low reactivity of heavy coke molecules does not explain the drastic change in selectivity. The beginning of their oxidation could indicate an increase in temperature in the DBD reactor. Indeed, the temperature rise is not an instantaneous phenomenon but requires several tens of minutes [35].

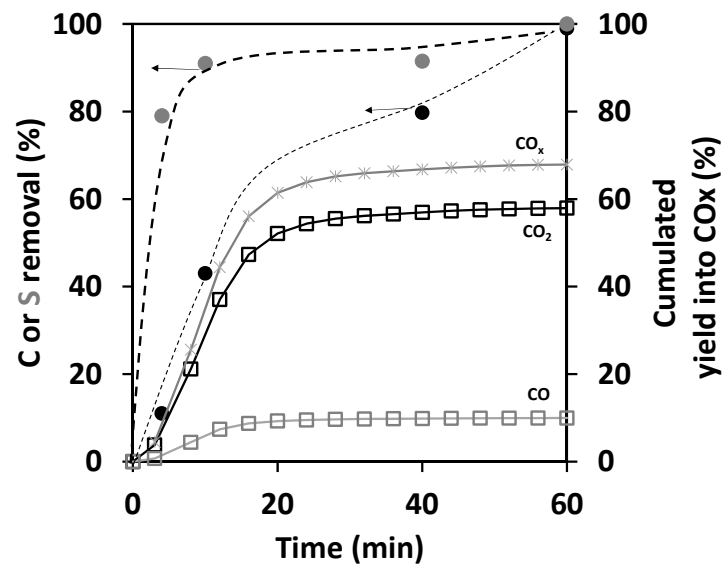


Figure 8. Time comparison of carbon (●) and sulfur (●) removal on the spent catalyst with the cumulated yields of CO (□), CO₂ (□), and their sum (✱). Experiments were performed at P = 7 W and 200 °C.

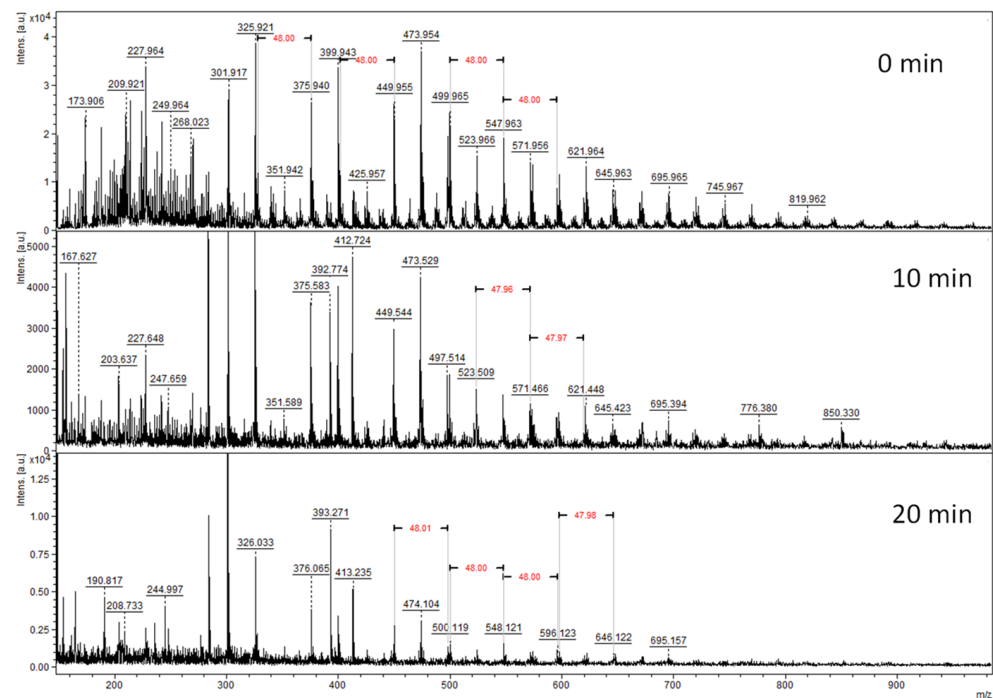


Figure 9. Time evolution of LDI-TOF/MS spectrum of the extracted coke by HF.

Figure 2 displays the evolution of the HDS catalyst XRD patterns during the plasma treatment. Al₂O₃ Bragg peaks are present regardless of the treatment time. After just 5 min, this of MoS₂ at $2\theta = 59^\circ$ disappears, while after 20 min, a peak at $2\theta = 26.5$, assigned to CoMoO₄, arises. It means that even at a low regeneration temperature, 200 °C, the plasma treatment induces some hot points, which lead to the formation of CoMoO₄. The temperature rise corresponds to the heavy coke elimination.

Moreover, the disappearance of MoS₂ slabs after only 5 min suggests that the refractory sulfur compounds to removal are the heavy sulfated coke molecules. TEM micrographs show significant textural and structural modifications of the catalyst during regeneration

treatment (Figure 3). After 10 min, the density and size of MoS₂ slabs size is divided by 10 and 5, respectively, and disappear after 40 min, correlating with the S removal.

After 5 min, MoS₂ Raman peaks at 380 and 407 cm⁻¹ disappear (Figure 4), consistent with TEM observations. From 40 min, the spectrum changes radically with the disappearance of the D and G bands and the appearance of many peaks. The peaks at 330, 370 at 330, 370, 819, 941, and 952/953 cm⁻¹, are assigned to CoMoO₄, (Table 2), consistent with XRD. The peaks at 1197, 483, 524, 692 cm⁻¹ indicate the formation of Co₃O₄, and these at 217, 351, 376, 573, 909, and 952 cm⁻¹ correspond either to CoMo₆ or AlMo₆. The water produced during coke combustion reacts with the catalyst and yields molybdenum aluminate.

These oxides indicate the significant changes in the oxidation states of species under regeneration by non-thermal plasma assisted with a moderated heating.

3. Materials and Methods

Catalyst: Spent industrial phosphorus-doped CoMoP/Al₂O₃ catalyst from a hydrodesulfurization unit after two years on stream was used as reference. Before use, soft coke is removed by washing with toluene in a Soxhlet type device. Reflux is maintained at 250 °C for 7 h after the catalyst is placed in a primary vacuum oven (30 mbar) at 150 °C for 3 h. The catalyst used in this study was crushed and sieved to obtain particles in the size range: 0.1–0.2 mm.

Catalyst regeneration: Catalyst regeneration under non-thermal plasma was performed in a cylindrical dielectric barrier discharge reactor (DBD reactor) placed in a furnace (Figure 10). The NTP reactor is composed of an alumina tube with an internal diameter of 4 mm, a stainless steel rod (1.16 mm) as the inner electrode, and a copper sheet as an external electrode (20 mm in length). A high voltage (HV) sinusoidal generator is used to generate plasma: A low-frequency generator (GBF) from TTI[®] model TG1010A is coupled to a signal amplifier from TREK[®] model 30/20 A. The deposited power was measured by the Q-U Lissajous method. The gas feed was composed of 20 vol% O₂ in He. The GHSV was fixed at 6000 h⁻¹, and 350 mg of catalyst was used per test. NTP treatments were carried out with an applied power of 7 W, at room temperature and 200 °C.

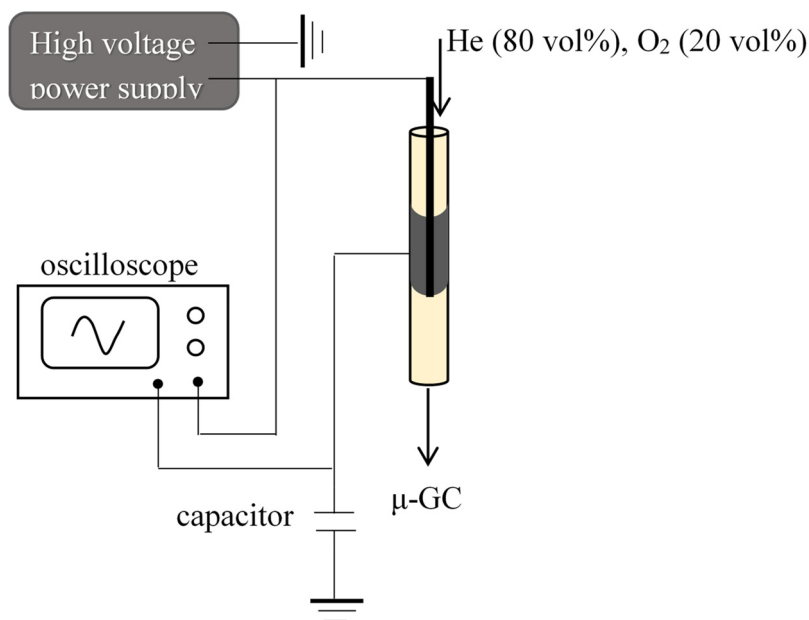


Figure 10. Dielectric barrier discharge plasma reactor.

At the exit of the reactor, the gas flow composition was determined by online gas chromatographic analysis using a Micro GC Varian CP 4900 equipped with a TCD detector and a “CO_x column”. The concentration in CO₂ and CO are measured, while other possible organic molecules (VOC) and water are trapped upstream of the micro GC

Catalyst characterization: X-Ray diffraction patterns of the catalysts were recorded using a Malvern Panalytical[®], Empyrean model diffractometer operating with Cu K 1 (radiation (λ) = 0.15406 nm) in the range of $10^\circ < 2\theta < 80^\circ$ with a step of 0.04° using a zero background holder with a 32 mm diameter.

Samples were characterized by transmission electronic microscopy (TEM) using a JEOL 2100 microscope equipped with a LaB6 filament operating at 200 kV and coupled to an Energy-dispersive X-ray detector (JEOL EDS JED 200). The samples were first prepared by ultrasonic dispersion in ethanol and then dropped onto a copper grid, previously covered with a carbon film.

Spent and treated by NTP catalysts were characterized by transmission electronic microscopy (TEM) using a Philips CM 120 microscope equipped with a LaB6 filament.

Raman spectroscopy is performed at room temperature using a HORIBA JOBIN YVON Labram HR800UV confocal Raman microscope equipped with a Peltier-cooled CCD detector. The excitation wavelength is 532 nm. The laser power delivered to the sample is 0.2 mW (using an optical density filter). The apparatus is equipped with an Olympus BXFM confocal microscope, which allows working in backscattering. A diffraction grating with 600 lines. mm^{-1} is used, and the confocal hole aperture is 200 μm . The spectral resolution is 1.5 cm^{-1} . The spectrometer is calibrated with a silicon standard. The LabSpec v.5 software allows the acquisition and processing of the results.

Coke characterization: The amount of carbon and sulfur were measured using a C.E. Instruments NA2100 PROTEIN elementary analyzer.

Prior to analysis, the spent catalyst was dissolved in 51 vol% hydrofluoric acid solution at room temperature for 20 min. HF was neutralized by a boric acid solution and sodium hydrogen carbonate. The low temperature of treatment by HF, the short contact time of the acid solution, and the coke components, and the minimal contact area between mineral and organic phases prevent coke composition changes.

The coke residue was extracted using CH_2Cl_2 . In all cases, the totality of coke appears as insoluble (black particles). The solid particles were recovered, dried, and weighted, and characterized by Laser Desorption/ionization-Time-of-Flight mass spectrometry (LDI-TOF/MS) [30] on a Bruker Daltonics Speed mass spectrometer in a reflectron positive mode where ions were generated by a 335 nm wavelength smart beam-laser. Analyses were performed using pulsed ion extraction (delay time 130 ns) at a scan rate of 2 kHz in the mass range between m/z 150 and 950. The laser power was adjusted slightly above the desorption/ionization process threshold, and the spectra resulted from 40,000 shots. The spectra presented in this paper include baseline correction and no signal smoothing.

4. Conclusions

The regeneration of an aged industrial hydrodesulfurization catalyst is possible when coupling non-thermal plasma with moderate heating. Indeed at 200°C , applying a low input power (7 W) removes the coke. Several phenomena, more or less rapid, operate during the regeneration treatment. From the beginning, MoS_2 slabs rapidly oxidize in molybdenum oxide, and after an extended period, due to a local increase of the temperature inside the DBD reactor, appears on the alumina surface, other oxides like Co_3O_4 , CoMo_6 , or AlMo_6 and also CoMoO_4 , species known to be refractory to sulfidation.

The coke consists of two families (i) “light” coke molecules with a molar weight ranging from 100 to $300 \text{ g}\cdot\text{mol}^{-1}$ and (ii) “hard” coke with heavy sulfated molecules having a molar weight up to $800 \text{ g}\cdot\text{mol}^{-1}$. We showed in this study that the “light” coke is oxidized into CO_2 , while the “hard” coke is partially and slowly transformed into volatile organic compounds. These species refractory to oxidation are removed when the temperature within the DBD reactor increases. The formation of hot spots leads to the formation of CoMoO_4 .

Under the experimental conditions used in this study, the NTP process assisted by a temperature of 200°C is able to remove the coke from an aged HDS catalyst but the kinetic is slow. The development of this technology involves the management of the treatment

time to prevent the formation of CoMo₄. Sequential experiments that turn-on and turn-off of the NTP or the associated oven should overcome the generation of hot spots and avoid the appearance of oxide refractory to sulfidation.

Author Contributions: Conceptualization, L.P.; methodology, L.P.; validation, C.B.-D. and L.P.; formal analysis, N.G. (Raman), M.T. (LDI/TOF); investigation, H.S.; resources, writing—original draft preparation, L.P. and H.S.; writing—review and editing, A.M.-B., E.D. and L.P.; supervision, C.B.-D. and L.P.; funding acquisition, J.T., T.H., L.P. All authors have read and agreed to the published version of the manuscript.

Funding: This research received no external funding.

Acknowledgments: The authors gratefully acknowledge IFPEN for its financial support. Hawraa Srour thanks the Lebanese University and IC2MP for the Ph.D. grant. The authors acknowledge financial support from the European Union (ERDF) and “Région Nouvelle Aquitaine”.

Conflicts of Interest: The authors declare no conflict of interest.

References

1. Sentek, J.; Krawczyk, K.; Młotek, M.; Kalczyńska, M.; Kroker, T.; Kolb, T.; Schenk, A.; Gericke, K.-H.; Schmidt-Szałowski, K. Plasma-catalytic methane conversion with carbon dioxide in dielectric barrier discharges. *Appl. Catal. B Environ.* **2010**, *94*, 19–26. [[CrossRef](#)]
2. Mizushima, T.; Matsumoto, K.; Sugoh, J.; Ohkita, H.; Kakuta, N. Tubular membrane-like catalyst for reactor with dielectric-barrier-discharge plasma and its performance in ammonia synthesis. *Appl. Catal. Gen.* **2004**, *265*, 53–59. [[CrossRef](#)]
3. Barakat, C.; Gravejat, P.; Guaitella, O.; Thevenet, F.; Rousseau, A. Oxidation of isopropanol and acetone adsorbed on TiO₂ under plasma generated ozone flow: Gas phase and adsorbed species monitoring. *Appl. Catal. B Environ.* **2014**, *147*, 302–313. [[CrossRef](#)]
4. Ayrault, C.; Barrault, J.; Blin-Simiand, N.; Jorand, F.; Pasquiers, S.; Rousseau, A.; Tatibouët, J.M. Oxidation of 2-heptanone in air by a DBD-type plasma generated within a honeycomb monolith supported Pt-based catalyst. *Catal. Today* **2004**, *89*, 75–81. [[CrossRef](#)]
5. Bogaerts, A.; Tu, X.; Whitehead, J.C.; Centi, G.; Lefferts, L.; Guaitella, O.; Azzolina-Jury, F.; Kim, H.-H.; Murphy, A.B.; Schneider, W.F.; et al. The 2020 plasma catalysis roadmap. *J. Phys. Appl. Phys.* **2020**, *53*, 443001. [[CrossRef](#)]
6. Li, J.; Ma, C.; Zhu, S.; Yu, F.; Dai, B.; Yang, D. A Review of Recent Advances of Dielectric Barrier Discharge Plasma in Catalysis. *Nanomaterials* **2019**, *9*, 1428. [[CrossRef](#)]
7. Liu, C.; Li, M.; Wang, J.; Zhou, X.; Guo, Q.; Yan, J.; Li, Y. Plasma methods for preparing green catalysts: Current status and perspective. *Chin. J. Catal.* **2016**, *37*, 340–348. [[CrossRef](#)]
8. Jia, L.Y.; Farouha, A.; Pinard, L.; Hedan, S.; Comparot, J.-D.; Dufour, A.; Ben Tayeb, K.; Vezin, H.; Batiot-Dupeyrat, C. New routes for complete regeneration of coked zeolite. *Appl. Catal. B Environ.* **2017**, *219*, 82–91. [[CrossRef](#)]
9. Lee, D.H.; Song, Y.-H.; Kim, K.-T.; Jo, S.; Kang, H. Current state and perspectives of plasma applications for catalyst regeneration. *Catal. Today* **2019**, *337*, 15–27. [[CrossRef](#)]
10. Eliasson, B.; Hirth, M.; Kogelschatz, U. Ozone Synthesis from Oxygen in Dielectric Barrier Discharges. *J. Phys. D: Appl. Phys.* **1987**, *20*, 1421. [[CrossRef](#)]
11. Khan, M.A.; Al-Jalal, A.A. Enhanced decoking of a coked zeolite catalyst using a glow discharge in Ar–O₂ gas mixture. *Appl. Catal. Gen.* **2004**, *272*, 141–149. [[CrossRef](#)]
12. Khan, M.A.; Al-Jalal, A.A.; Bakhtiari, I.A. “Decoking” of a “coked” zeolite Catalyst in a Glow Discharge. *Anal. Bioanal. Chem.* **2003**, *377*, 89–96. [[CrossRef](#)] [[PubMed](#)]
13. Kim, M.; Jeoung, J.; Kim, J.; Ha, K.-S. Regeneration of deactivated H-ZSM-5 for aromatization by dielectric barrier discharge plasma. *Appl. Catal. Gen.* **2019**, *575*, 214–222. [[CrossRef](#)]
14. Hafez Khiabani, N.; Fathi, S.; Shokri, B.; Hosseini, S.I. A novel method for decoking of Pt–Sn/Al₂O₃ in the naphtha reforming process using RF and pin-to-plate DBD plasma systems. *Appl. Catal. Gen.* **2015**, *493*, 8–16. [[CrossRef](#)]
15. Pinard, L.; Ayoub, N.; Batiot-Dupeyrat, C. Regeneration of a Coked Zeolite via Nonthermal Plasma Process: A Parametric Study. *Plasma Chem. Plasma Process.* **2019**, *39*, 929–936. [[CrossRef](#)]
16. Astafan, A.; Batiot-Dupeyrat, C.; Pinard, L. Mechanism and Kinetic of Coke Oxidation by Nonthermal Plasma in Fixed-Bed Dielectric Barrier Reactor. *J. Phys. Chem. C* **2019**, *123*, 9168–9175. [[CrossRef](#)]
17. Srour, H.; Alnaboulsi, A.; Astafan, A.; Devers, E.; Toufaily, J.; Hamieh, T.; Pinard, L.; Batiot-Dupeyrat, C. Elimination of Coke in an Aged Hydrotreating Catalyst via a Non-Thermal Plasma Process: Comparison with a Coked Zeolite. *Catalysts* **2019**, *9*, 783. [[CrossRef](#)]
18. Topsøe, H.; Clausen, B.S.; Candia, R.; Wivel, C.; Mørup, S. In Situ Mössbauer Emission Spectroscopy Studies of Unsupported and Supported Sulfided Co Mo Hydrodesulfurization Catalysts: Evidence for and Nature of a Co Mo S Phase. *J. Catal.* **1981**, *68*, 433–452. [[CrossRef](#)]
19. Yoshimura, Y.; Sato, T.; Shimada, H.; Matsubayashi, N.; Imamura, M.; Nishijima, A.; Yoshitomi, S.; Kameoka, T.; Yanase, H. Oxidative Regeneration of Spent Molybdate and Tungstate Hydrotreating Catalysts. *Energy Fuels* **1994**, *8*, 435–445. [[CrossRef](#)]

20. Srouf, H.; Devers, E.; Mekki-Berrada, A.; Toufaily, J.; Hamieh, T.; Batiot-Dupeyrat, C.; Pinard, L. Regeneration of an aged hydrodesulfurization catalyst: Conventional thermal vs non-thermal plasma technology. *Fuel* **2021**, *306*, 121674. [[CrossRef](#)]
21. Guisnet, M.; Ribeiro, F.R. Characterization of Deactivating Species. In *Deactivation and Regeneration of Zeolite Catalysts*; Imperial College Press: London, UK, 2011; pp. 51–81. [[CrossRef](#)]
22. Cerqueira, H.S.; Sievers, C.; Joly, G.; Magnoux, P.; Lercher, J.A. Multitechnique Characterization of Coke Produced during Commercial Resid FCC Operation. *Ind. Eng. Chem. Res.* **2005**, *44*, 2069–2077. [[CrossRef](#)]
23. Bauer, F.; Chen, W.H.; Bilz, E.; Freyer, A.; Sauerland, V.; Liu, S.B. Surface modification of nano-sized HZSM-5 and HFER by pre-coking and silanization. *J. Catal.* **2007**, *251*, 258–270. [[CrossRef](#)]
24. Kimura, N.; Iwanami, Y.; Koide, R.; Kudo, R. Characterization of coke, or carbonaceous matter, formed on CoMo catalysts used in hydrodesulfurization unit in oil refinery. *Jpn. J. Appl. Phys.* **2017**, *56*, 06GE08. [[CrossRef](#)]
25. Callejas, M.A.; Martinez, M.T.; Blasco, T.; Sastre, E. Coke Characterisation in Aged Residue Hydrotreating Catalysts by Solid-State ¹³C-NMR Spectroscopy and Temperature-Programmed Oxidation. *Appl. Catal. Gen.* **2001**, *218*, 181–188. [[CrossRef](#)]
26. Koh, J.H.; Lee, J.J.; Kim, H.; Cho, A.; Moon, S.H. Correlation of the deactivation of CoMo/Al₂O₃ in hydrodesulfurization with surface carbon species. *Appl. Catal. B Environ.* **2009**, *86*, 176–181. [[CrossRef](#)]
27. Le Minh, C.; Jones, R.A.; Craven, I.E.; Brown, T.C. Temperature-Programmed Oxidation of Coke Deposited on Cracking Catalysts: Combustion Mechanism Dependence. *Energy Fuels* **1997**, *11*, 463–469. [[CrossRef](#)]
28. Vogelaar, B.M.; van Langeveld, A.D.; Eijssbouts, S.; Moulijn, J.A. Analysis of coke deposition profiles in commercial spent hydroprocessing catalysts using Raman spectroscopy. *Fuel* **2007**, *86*, 1122–1129. [[CrossRef](#)]
29. Ferrari, A.C.; Robertson, J. Interpretation of Raman spectra of disordered and amorphous carbon. *Phys. Rev. B* **2000**, *61*, 14095–14107. [[CrossRef](#)]
30. Cançado, L.G.; Takai, K.; Enoki, T.; Endo, M.; Kim, Y.A.; Mizusaki, H.; Jorio, A.; Coelho, L.N.; Magalhães-Paniago, R.; Pimenta, M.A. General equation for the determination of the crystallite size *L*_a of nanographite by Raman spectroscopy. *Appl. Phys. Lett.* **2006**, *88*, 163106. [[CrossRef](#)]
31. Jawhari, T.; Roid, A.; Casado, J. Raman spectroscopic characterization of some commercially available carbon black materials. *Carbon* **1995**, *33*, 1561–1565. [[CrossRef](#)]
32. Bui, N.-Q.; Geantet, C.; Berhault, G. Maleic acid, an efficient additive for the activation of regenerated CoMo/Al₂O₃ hydrotreating catalysts. *J. Catal.* **2015**, *330*, 374–386. [[CrossRef](#)]
33. Gandubert, A.D.; Legens, C.; Guillaume, D.; Rebours, S.; Payen, E. X-ray Photoelectron Spectroscopy Surface Quantification of Sulfided CoMoP Catalysts—Relation Between Activity and Promoted Sites—Part I: Influence of the Co/Mo Ratio. *Oil Gas. Sci. Technol. Rev. L'IFP* **2007**, *62*, 79–89. [[CrossRef](#)]
34. Pinard, L.; Hamieh, S.; Canaff, C.; Madeira, F.F.; Batonneau-Gener, I.; Maury, S.; Delpoux, O.; Ben Tayeb, K.; Pouilloux, Y.; Vezin, H. Growth mechanism of coke on HBEA zeolite during ethanol transformation. *J. Catal.* **2013**, *299*, 284–297. [[CrossRef](#)]
35. Sadat, H.; Dubus, N.; Pinard, L.; Tatibouet, J.M.; Barrault, J. Conduction heat transfer in a cylindrical dielectric barrier discharge reactor. *Appl. Therm. Eng.* **2009**, *29*, 1259–1263. [[CrossRef](#)]